

## Residual seismic performance of steel bridges under earthquake sequence

Zhanzhan Tang<sup>1,2</sup>, Xu Xie<sup>\*1</sup> and Tong Wang<sup>1</sup>

<sup>1</sup>Department of Civil Engineering, Zhejiang University, Zhejiang, 310058, China

<sup>2</sup>College of Civil Science and Engineering, Yangzhou University, Jiangsu, 225127, China

(Received December 30, 2014, Revised August 23, 2016, Accepted September 6, 2016)

**Abstract.** A seismic damaged bridge may be hit again by a strong aftershock or another earthquake in a short interval before the repair work has been done. However, discussions about the impact of the unrepaired damages on the residual earthquake resistance of a steel bridge are very scarce at present. In this paper, nonlinear time-history analysis of a steel arch bridge was performed using multi-scale hybrid model. Two strong historical records of main shock-aftershock sequences were taken as the input ground motions during the dynamic analysis. The strain response, local deformation and the accumulation of plasticity of the bridge with and without unrepaired seismic damage were compared. Moreover, the effect of earthquake sequence on crack initiation caused by low-cycle fatigue of the steel bridge was investigated. The results show that seismic damage has little impact on the overall structural displacement response during the aftershock. The residual local deformation, strain response and the cumulative equivalent plastic strain are affected to some extent by the unrepaired damage. Low-cycle fatigue of the steel arch bridge is not induced by the earthquake sequences. Damage indexes of low-cycle fatigue predicted based on different theories are not exactly the same.

**Keywords:** steel arch bridge; earthquake sequence; multi-scale hybrid model; seismic damage; residual seismic capacity; low-cycle fatigue

### 1. Introduction

Numerous historical earthquake records indicate that a strong main shock is often preceded by foreshocks and followed by aftershocks, forming foreshocks-main shock-aftershocks sequence-type ground motions (e.g., Alliard 2006, Kim *et al.* 2010, Chen *et al.* 2002). The magnitudes and frequencies of the aftershocks are related to the main shock (e.g., Li *et al.* 2007, Sakai *et al.* 2014). Sunasaka *et al.* (1993) summarized the probability density function of the aftershock magnitudes as Eq. (1)

$$f_{M_a}(m_a) = \frac{\beta e^{-\beta m_a}}{e^{-3.0\beta} - e^{-\beta M_m}} \quad (1)$$

---

\*Corresponding author, Professor, E-mail: xiexu@zju.edu.cn

In the equation,  $M_a$  and  $M_m$  are the magnitudes of the main shock and the aftershock, respectively.  $m_a$  is the state variable of the aftershock magnitude,  $\beta$  is a constant related to  $M_m$  and greater than zero,  $f_{M_a}$  represents the probability density of  $M_a$ . This equation demonstrates that a strong aftershock may occur after a very strong main shock. For example, it can be inferred from Eq. (1) that, the probability exceeds 20% when the magnitude of the strongest aftershock is only 0.5 smaller than the main one.

Historical seismic records can also reflect the same phenomena mentioned above. For instance, the magnitude of 1999 Chi-chi main shock was M7.3, while the strongest aftershock was M6.8 (Kim *et al.* 2010). The magnitudes of 2004 Niigata main shock and its strongest aftershock were M6.8 and M6.5, respectively (Japan Meteorological Agency 2004). Moreover, though the energy released by an aftershock is smaller than that released by the main shock, the peak ground acceleration (PGA) of the aftershock sometimes is very large (e.g., Yeo *et al.* 2009, Li *et al.* 2014, Zhang *et al.* 2013, Zhao *et al.* 2010). For example, the strongest aftershock in the 1992 American Landers earthquake happened 10 hours after the main one, but its PGA which recorded at the same station was greater than the main shock (Li *et al.* 2014). The PGA of the aftershock in the 2004 Niigata earthquake even reached to 2.0 g (recorded in Kawaguchi station, g is the acceleration of gravity), and it was evidently larger than the PGA of the main shock since the hypocenter locations of each earthquake were not exactly the same (Japan Meteorological Agency 2004).

In addition, several strong earthquakes separated by short intervals of time may happen in the same area (e.g., Amadio *et al.* 2003, Faisal *et al.* 2013). For example, two strong earthquakes hit Berlongfer (India) in 1988 and 1990. Two major earthquakes of magnitudes of M7.6 and M7.2 with an interval of 13 minutes occurred in Lancang and Gengma County, China in 1988 (Chen *et al.* 2014).

In such cases, the steel bridges, already damaged after the first earthquake, may become completely inadequate due to damage accumulation during a strong aftershock or a second earthquake. Therefore, it is very significant to take the unrepaired seismic damage into account when evaluating the residual capacity of a bridge against another earthquake. Seismic damages of a steel bridge can be mainly classified into several types as follows according to seismic disasters and laboratory tests (Usami *et al.* 2009, Ge *et al.* 2011, 2012a, 2013, 2014): local buckling of the cross-section caused by compression or shear, overall instability, excessive residual deformation caused by exaggerated plastic strain, and fracture failure caused by low-cycle fatigue. Among these seismic damage types, the residual deformation and low-cycle fatigue damage may accumulate to their ultimate value for a steel bridge undergoing multiple strong earthquakes. At present all the seismic design codes in the world deal very carefully with seismic safety of a bridge, but not involve with residual seismic capacity to resist another earthquake (e.g., AASHTO 2009, California Department of Transportation 2004, Japan Road Association 2002, Chinese Ministry of Communications 2008).

So far, only a few works have been done on seismic performance of steel bridges undergoing earthquake sequence. For example, in order to examine the effect of steel shear panel dampers under earthquake sequence, Ge *et al.* (2012b) simulated the main shock-aftershock sequence by the repetition of a strong main shock. In their study, the fiber model was utilized for the dynamic analysis, and the performance requirements of the steel dampers were concluded. Xie *et al.* (2012) investigated the residual capacity of a main shock-damaged steel suspension bridge to withstand an aftershock using fiber model. Through the comparison of the structural response (e.g., the equivalent plastic strain, the strain response), they reported that the assessment of seismic damage caused by earthquake sequence can be determined by the superposition of damage under

independent action of each seismic excitation. However, the adopted fiber model was unable to take into consideration the stress concentration and local deformation of the cross-section. As a steel bridge usually consists of many thin-walled components, local deformation of a thin-walled cross-section is very common under the action of strong ground motions. Therefore, it is very significant for a FE model to be able to consider the local deformation when conducting structural seismic response analysis.

In this paper, real main shock-aftershock sequences records were taken as the input ground motions. Nonlinear time-history dynamic analysis of a steel arch bridge using fine multi-scale hybrid model was conducted first. Through comparing the residual local deformation, the strain response and the low-cycle fatigue damage index, the influence of existing seismic damage on the residual earthquake resistance of the steel bridge was studied carefully then. Finally, low-cycle fatigue failure of the steel bridge under earthquake sequence was evaluated based on different theories.

## 2. Seismic damage indexes of a steel bridge

According to the seismic damage types of steel bridges, the dynamic stability and bearing capacity, the post-earthquake serviceability and reparability, low-cycle fatigue are some important contents for seismic safety checking. Most of the safety checking work can be done directly through the dynamic analysis with a fine numerical model, except for the low-cycle fatigue failure. For example, local and overall buckling can be fully considered automatically when the nonlinear time-history analysis procedure is able to take into account both the geometric and material nonlinearities. The maximum seismic displacement response, residual deformation, strain response, etc. can be obtained by a fine FE model after the dynamic analysis. Low-cycle fatigue failure is very hard to be directly determined from a numerical model.

Many researches have been done on low-cycle fatigue of the structural steel so far (Ge *et al.* 2011, 2012a, 2013, 2014, Kanvinde *et al.* 2007, Kiran *et al.* 2015). Based on the Miner's rule and Manson-Coffin relation, low-cycle fatigue is cracking damage of the steel material caused by cumulative plastic strain under cyclic loads. The cumulative damage index  $D$  is expressed as (e.g., Ge *et al.* 2014)

$$D = C \sum_{i=1}^n (\varepsilon_{pi})^m \quad (2)$$

where  $\varepsilon_{pi}$  is the plastic strain range of every half load loop shown in Fig. 1(a).  $C$  and  $m$  are material constants, they can be taken as 9.69 and 1.86 for structural steel, respectively (Ge *et al.* 2014). In Fig. 1(a),  $\sigma$  and  $\varepsilon$  are the stress and strain of the material, respectively. When  $D$  exceeds 1.0, the crack failure occurs.

Based on void growth theory, low-cycle fatigue is cracking damage induced by the development of microvoid which involves three stages: microvoid nucleation, void growth and void coalescence (Chi *et al.* 2006, Kanvinde *et al.* 2007, Liao *et al.* 2012, Kiran *et al.* 2015). The dilation and elongation of the microvoids is related to the stress triaxiality  $\sigma_m$  in the damage area. Kanvinde *et al.* (2007) proposed a practical formula to evaluate the low-cycle fatigue for steel material under cyclic loads.

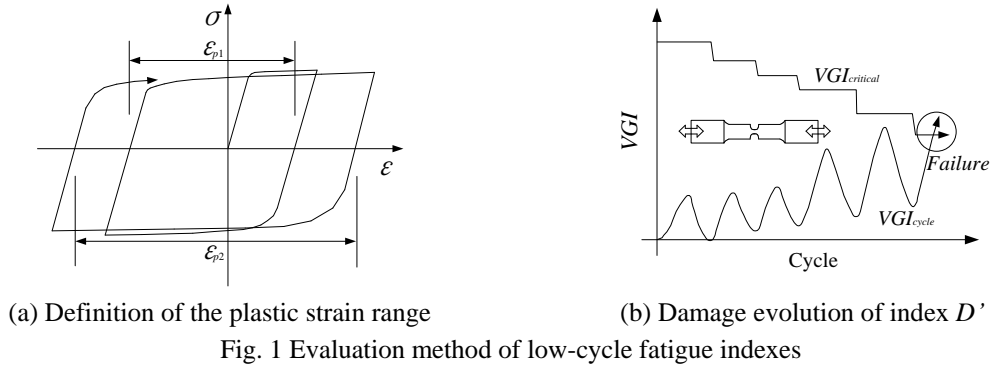


Fig. 1 Evaluation method of low-cycle fatigue indexes

$$\left\{ \begin{array}{l}
 D' = VGI_{critical} - VGI_{cycle} \\
 VGI_{cycle} = \sum_{tensile} \int_{\varepsilon_1}^{\varepsilon_2} \exp(|1.5\sigma_m|) d\varepsilon_p - \sum_{compressive} \int_{\varepsilon_1}^{\varepsilon_2} \exp(|1.5\sigma_m|) d\varepsilon_p \\
 VGI_{critical} = VGI_{monotonic} \exp(-\lambda' \varepsilon_{eq+}) \\
 \sigma_m = \frac{\frac{1}{3}(\sigma_1 + \sigma_2 + \sigma_3)}{\sqrt{\frac{1}{2}[(\sigma_1 - \sigma_2)^2 + (\sigma_2 - \sigma_3)^2 + (\sigma_3 - \sigma_1)^2]}}
 \end{array} \right. \quad (3)$$

In Eq. (3),  $D'$  is the damage index of low-cycle fatigue,  $VGI$  means the void growth index in the damage area.  $VGI_{monotonic}$  and  $\lambda'$  are the parameters related to the material (Liao *et al.* 2012).  $\varepsilon_{eq+}$  is the equivalent plastic strain at the beginning at the last tensile cycle,  $\sigma_1$ ,  $\sigma_2$  and  $\sigma_3$  are the principle stresses where the crack occurs. As shown in Fig. 1(b), when  $D' < 0$ , the void growth index  $VGI_{cycle}$  is greater than the critical value  $VGI_{critical}$ , the crack failure occurs.

It can be seen that, the damage index  $D'$  in Eq. (3) won't increase when the material is under a compression state, which is different with the evolution procedure of damage index  $D$  in Eq. (2).

### 3. The multi-scale hybrid model that can consider the local deformation

#### 3.1 Shell mesh length in a multi-scale hybrid model

Numerical model is widely used for dynamic analysis of structural design at present. The accuracy of the fiber model will decrease greatly when a steel structure is under an extensive seismic damage state (Tang *et al.* 2014, Zhao *et al.* 2014). However, the multi-scale hybrid model, which consists of both fiber and shell elements in a FE model, can overcome the drawback since it can take into account the local deformation and strain concentration of steel plates. Also, this model has been demonstrated to possess a lower computational cost and a higher accuracy, especially for seismic performance evaluation of steel structures (e.g., Kakiuchi *et al.* 2009, Tang *et al.* 2014, Zhao *et al.* 2014).

Generally, the seismic damage areas are clustered at some certain parts in a steel structure. Such as the portal frame shown in Fig. 2, in which six damaged segments represented as A~F exist. In

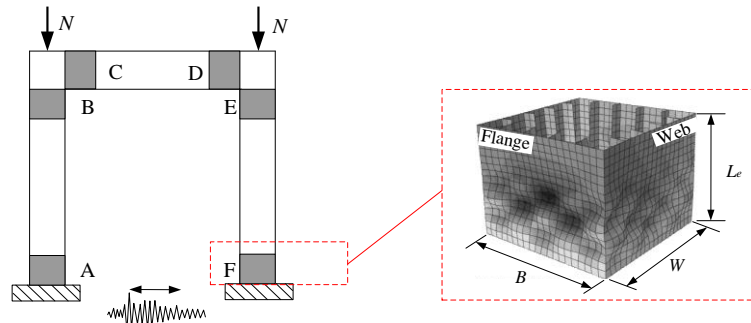


Fig. 2 Seismic damaged segments and local deformation form of the portal structure

the figure,  $W$  is the width of the web plate,  $B$  is the breadth of the flange,  $N$  is the axial force of the column. In order to achieve a reasonable length of shell mesh part in a multi-scale hybrid model, Tang *et al.* (2015) studied the impact of design parameters (e.g., the width-thickness ratio of the stiffened plate  $R_r$ , the slenderness ratio of the member  $\lambda$ , the breadth-width ratio of the cross section  $W/B$ , the diaphragm distance and section breadth ratio  $\alpha$ , axial compression ratio  $N/N_y$ ). For more information about these parameters, please see the Japanese code 2002 and Tang *et al.* (2015) on the length of seismic damage zone. A practical formula Eq. (4) of a fitted curve was summarized through the parametric study then. In the equation,  $L_e$  is the essential length ratio defined as the ratio of the shell mesh length to the flange width. When constructing a multi-scale hybrid model, the shell mesh length at the damage zone can be determined conservatively by Eq. (4)

$$\begin{cases} L_e = -2.2\phi + 0.46 \geq 0.4 \\ \phi = \alpha(R_r^{2.5} - 0.4)(N/N_y + 0.05)^{0.15}, \alpha < 1.0 \\ \phi = (R_r^{2.5} - 0.4)(N/N_y + 0.05)^{0.15}, \alpha \geq 1.0 \end{cases} \quad (4)$$

### 3.2 Effective failure areas for strain averaging

Strain response is one of the most significant indexes to describe and represent seismic damage degree of a steel bridge. Since a single point on the entire structure with the maximum strain response seems to be not so representative and typical, average strain  $\varepsilon_a$  over the excitation history is then adopted for safety control according to the Japanese code (Japan Road Association 2002). The effective failure areas for the strain averaging are critical locations that possibly to fail under seismic loads. The effective failure length  $L_\theta$  is determined due to the local buckling zone observed in experiments (e.g.,  $0.7B$ ). However,  $0.7B$  is a very rough length for strain response to average since some of the important information is omitted, such as local buckling and stress concentration of the steel plates. Therefore, smaller effective failure area may be more reasonable for shell mesh parts. Fig. 3 shows the local deformation forms of the cross-section in the portal structure shown in Fig. 2. Suppose that all the local deformations of the steel plates are sinusoidal waveform,  $1/\sqrt{2}$  times of the half wave length  $L$  in both the longitudinal and transverse directions is chosen in this paper as the effective failure area. It is necessary to declare here that further study is still needed for a reasonable effective failure area on the shell mesh parts.

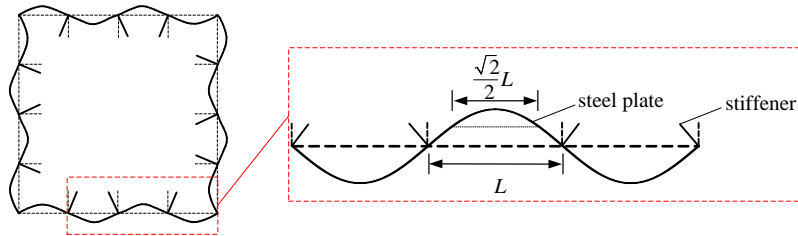


Fig. 3 Local deformation form of the stiffened steel plates and the effective failure area

### 3.3 The bridge structure

Fig. 4 shows the schematic view of the bridge with a span length of 130 m. In order to improve the stability of the main arch ribs, two secondary arch ribs with an inclined angle of  $17.5^\circ$  are connected at the outside of the two main ones. All the arches are fixed at their feet, and the width of the bridge deck is 50 m.

The stiffened rectangular sections are adopted for the tie beams and arch ribs as shown in Fig. 5. And the I-type sections are used as the transverse beams, the orthotropic plate is adopted for the bridge deck. The arch ribs have variable cross-sections, the thickness of the flanges and webs change from 21 mm and 26 mm at the arch spring to 20 mm at the arch crown for the main arch ribs, while the plate thickness is 8mm for both the secondary arch ribs and the tie beams.

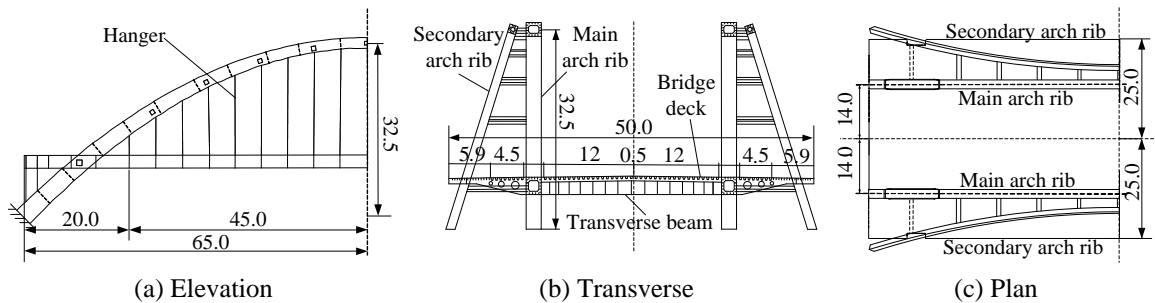


Fig. 4 The overview of the bridge (Unit: m)

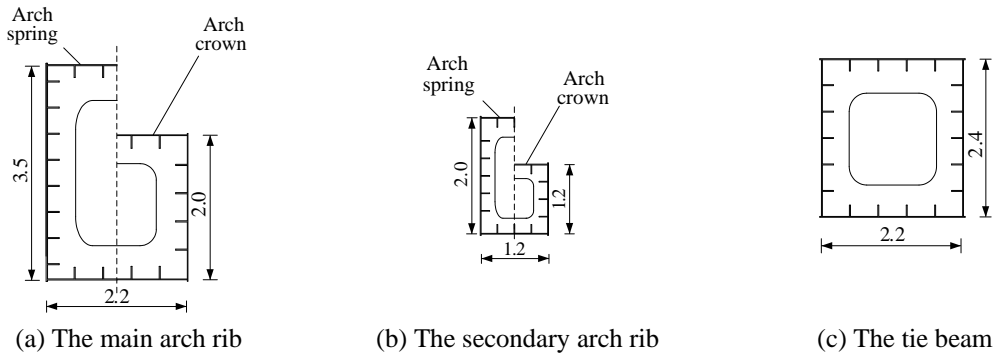


Fig. 5 Cross-sections of some main members of the bridge (Unit: m)

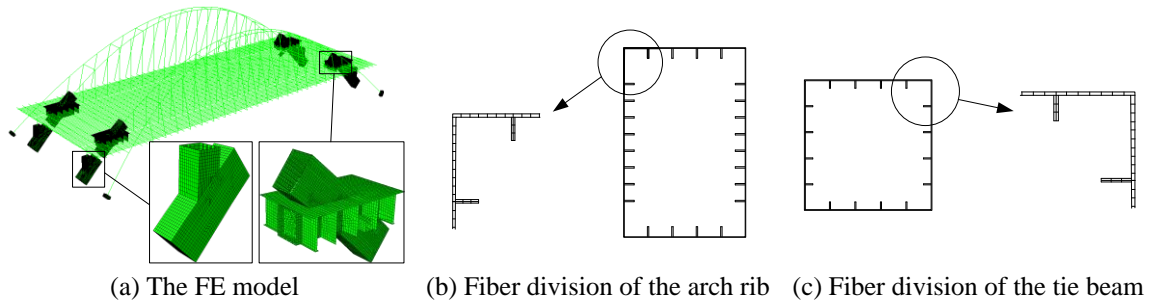


Fig. 6 Multi-scale hybrid model of the bridge and fiber division of some members

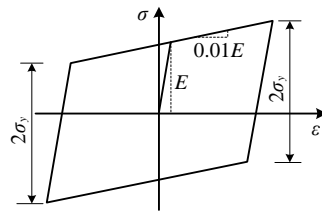


Fig. 7 Stress-strain relationship of the steel material

### 3.4 Analytical model of the steel bridge

Fig. 6 shows the multi-scale hybrid model of the bridge which is constructed based on Eq. (4). Also, the transverse divisions of some cross sections for fiber elements are shown in the figure. In the numerical model, the hangers are modeled by truss elements, the slight or no damaged parts are modeled by fiber elements. While the anticipated severe seismic damaged areas, e.g., the joints of the main arch ribs and girders, arch springs (Tang *et al.* 2014, Usami *et al.* 2005, Yamao *et al.* 2010) are modeled by fine shell elements. The total elements number of the whole bridge is 80444. The sectional fibers were 208 in number for both the main and secondary arch ribs, while 145 in number for both the tie beams and columns.

The finite element model in this paper is constructed using the commercial FE package ABAQUS 6.10. A bilinear stress-strain behavior with a kinematic hardening law shown in Fig. 7 is assumed for the structural steel material. In the figure,  $\sigma_y$  is the yield stress of the material. The Young's modulus  $E$  is  $2.06 \times 10^5$  MPa and the modulus after the yield point  $E'$  is taken as 1% of the initial one in consideration of the hardening effect. The Poisson's ratio  $\mu$  is 0.3. Besides, the yield stress of the hangers is 1670 MPa and its Young's modulus is  $2.0 \times 10^5$  MPa.

## 4. The input earthquake sequences and the main shock-induced damages

### 4.1 The input earthquake sequences

Dynamic analysis was carried out using the 1999 Chi-chi earthquake recorded near the Sun Moon Lake and the 2004 Niigate earthquake recorded in Kawaguchi as the input seismic loads. It should be noted that all the ground motions are unrelated to the actual bridge seismic design, they

are selected just to ensure the occurrence of severe seismic damage. Fig. 8 shows the acceleration waves and acceleration response spectra of the two earthquake sequences. In the figure,  $S_a$  is the spectral value of the acceleration. The PGA in EW direction of Chi-chi and Niigata waves are  $9.87 \text{ m/s}^2$  and  $16.76 \text{ m/s}^2$ , respectively. It can be seen from the response spectra that both of the two earthquakes have a higher intensity in their EW directions when the damping ratio is taken as 5%. The PGAs of the aftershocks for Chi-chi and Niigata earthquakes are 0.31 and 0.19 times of the main shocks in EW direction, respectively. To investigate the seismic damages under different levels of the bridge, the PGAs of the aftershock are respectively adjusted to 0.4, 0.6, 0.8 and 1.0 times of the main shock taking the EW direction as datum using incremental dynamic analysis method (Vamvatsikos *et al.* 2004). Thus, several new earthquake sequences are created to form several new load cases. For convenience, aftershock A (the original one), aftershock B, aftershock C, aftershock D and aftershock E are utilized to represent and distinguish the aftershocks with different intensities.

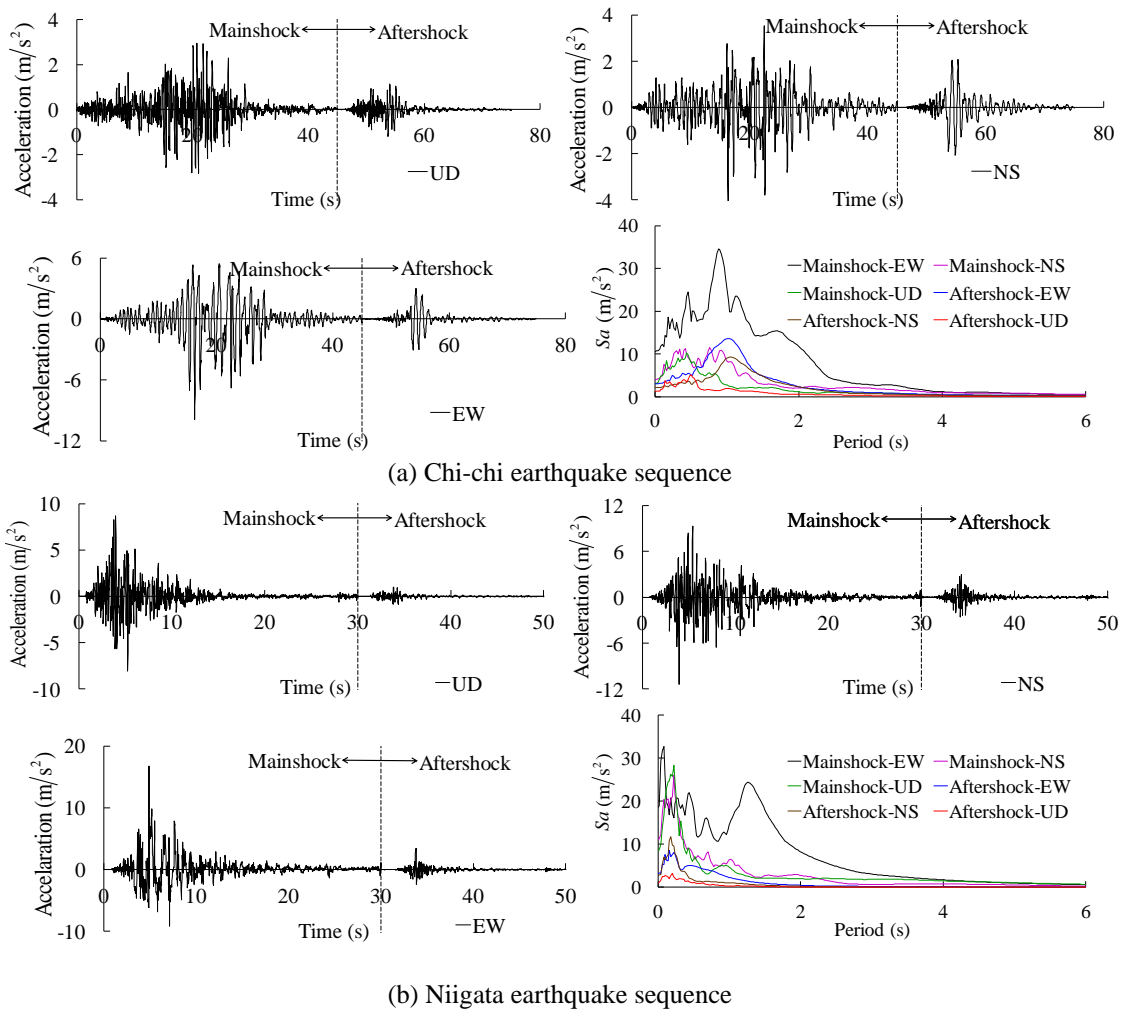


Fig. 8 The input earthquakes and their acceleration response spectra

4.2 Seismic damages caused by the main shock

As the steel arch bridge shows a good seismic performance and the main inertial force of the structure is in the bridge deck, severe seismic damages are observed at the arch springs and the intersections of the tie beams and arch ribs. Fig. 9 shows the specific seismic damage areas, from which we can see that seismic damage hasn't exceeded the shell mesh zones. The plastic region has penetrated throughout the whole section of the arch spring, while the structure still possesses a good seismic performance.

The most significant damage is observed at the intersection of the arch rib and the tie beam on the structure. Fig. 10 shows the hysteretic curve of the average stress-strain at the intersections, seismic damage caused by Chi-chi main shock is more serious than that caused by Niigata main shock. As large overall residual deformation is not observed, Fig. 11 only shows the residual local deformations caused by Chi-chi main shock at the damage areas. The rainbow spectrum utilized here is just to present the concavity or convexity of the plate, the shades of the color cannot express exactly how the steel plate has deformed. The magnitudes of these residual deformations at the arch spring and joint are  $B/82$  and  $B/143$ , respectively ( $B$  is the sectional flange breadth).

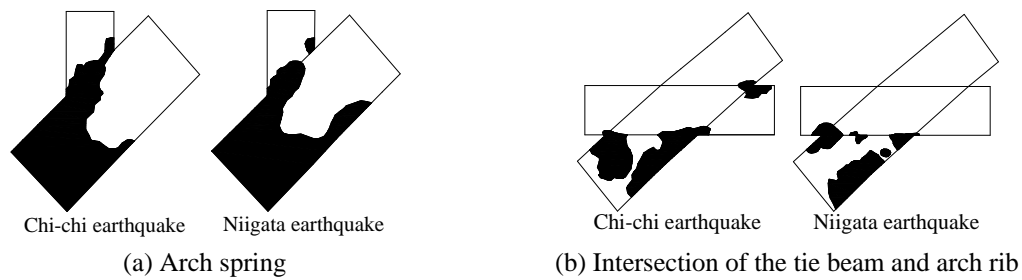


Fig. 9 The size of the main shock-induced seismic damage area

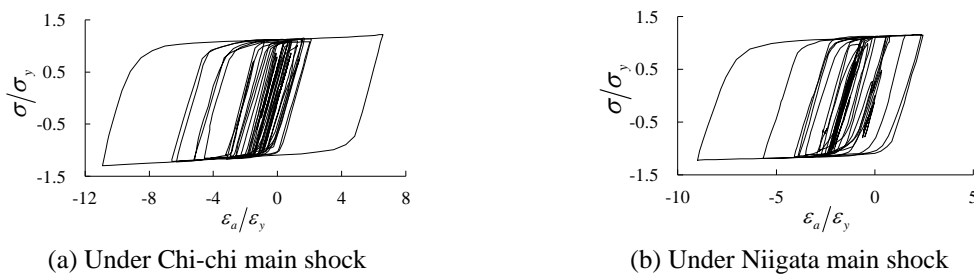


Fig. 10 Stress-strain history at the intersection of the arch rib and the tie beam

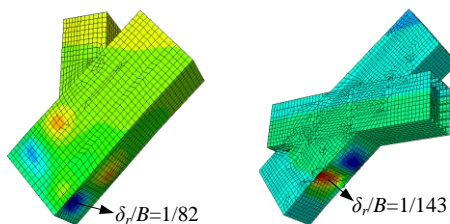


Fig. 11 The residual local deformation under the Chi-chi main shock

## 5. Effects of the unrepaired damage on the residual seismic performance

Nonlinear time-history analyses in this section were performed twice with aftershock as the input ground motions. The first time of the analysis was carried out for the undamaged structure, while the second time was carried out for the main shock-damaged structure. Through the comparison of the structural seismic response in these two cases, the effect of the unrepaired damage can be obtained. The “Restart” function provided by the software ABAQUS was adopted in the calculation procedure.

### 5.1 Seismic displacement response

Fig. 12 shows the comparison of displacement-history curves for the damaged and undamaged structure undergoing aftershock only. Since similar results are obtained, only the results induced by aftershock E are shown in this section. As it can be seen, the unrepaired seismic damage has a very small effect on both the maximum and the overall residual displacements of the structure under an aftershock. This indicates the overall stiffness does not deteriorate due to the unrepaired seismic damages.

### 5.2 Seismic strain response and the equivalent plastic strain

Fig. 13 shows the average strain response and the equivalent plastic strain of the damaged areas caused by the aftershock E.  $\varepsilon_{eq}$  is the average equivalent plastic strain that considers the effect of the main shock-induced damage, while  $\varepsilon_{eq}'$  is the average equivalent plastic strain of an undamaged bridge.  $\varepsilon_{pm}$  and  $\varepsilon_{pm}'$  are the the maximum ranges of the average strain response for the damaged and undamaged bridge, respectively. It is noted that the main shock-induced damages affected somehow the seismic strain response of the structure under the aftershock. In most cases, the increments of both the equivalent plastic strain and the strain range are less than 10% when consider the impact of the main shock-induced damage.

### 5.3 Seismic residual local deformation

As local deformations of the steel plates are more obvious caused by Chi-chi earthquake, the comparison is only carried out with deformations at the damage areas induced by this earthquake. Fig. 14 shows the residual deformations  $\delta_r$  caused by aftershock E only. The rainbow spectrum is utilized just to distinguish visually the inward or outward of the relative deformation, it cannot

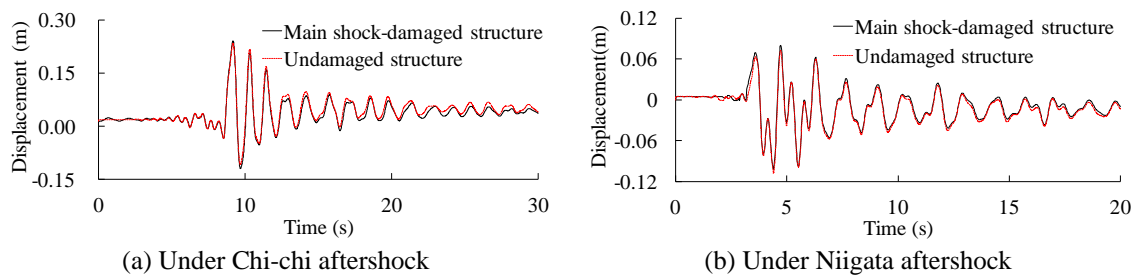
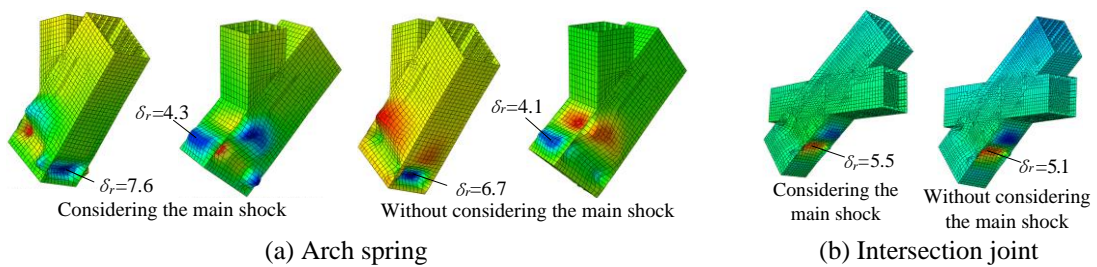
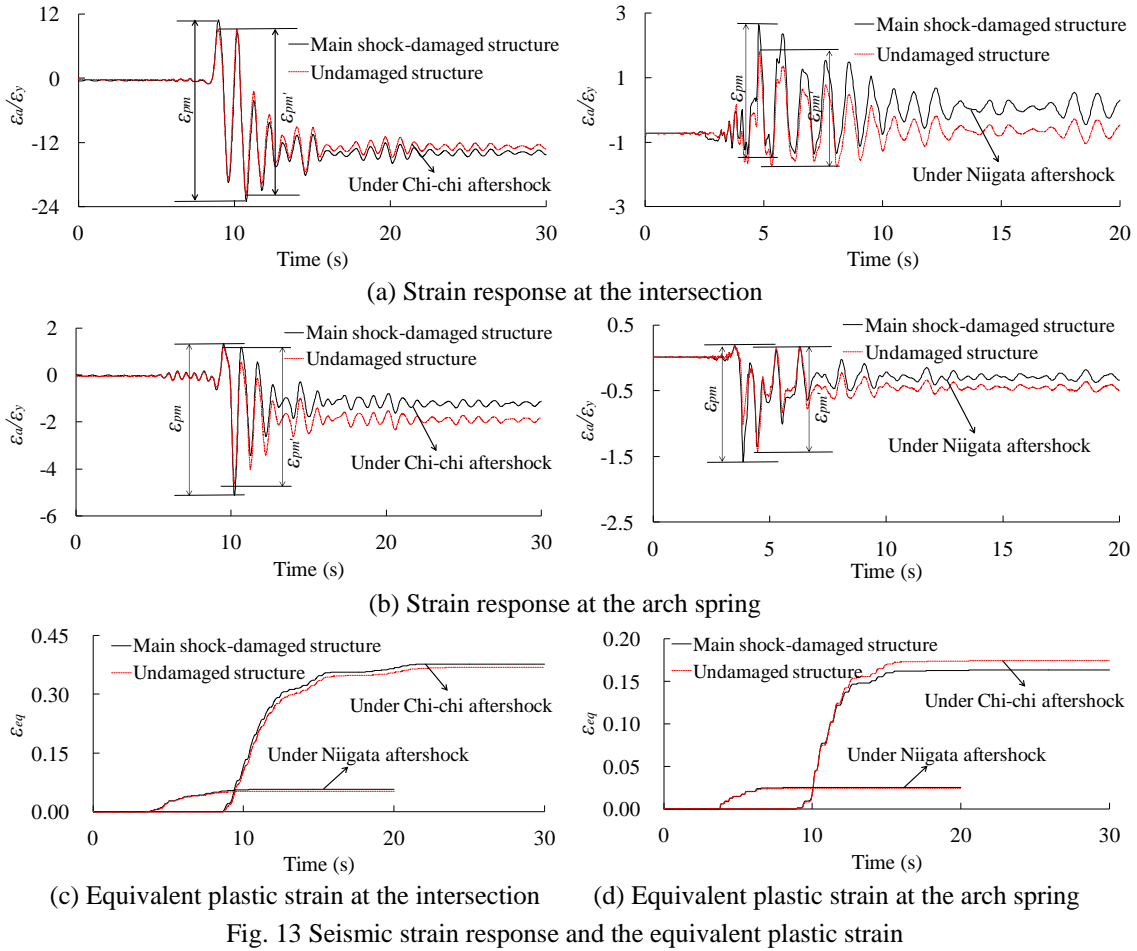


Fig. 12 The longitudinal displacement response of the 1/4-span arch rib



express exactly how the steel plate has deformed. As shown in the figure, the unrepaired damage has enlarged the residual local deformation by 13.4% and 7.8% for the arch spring and the joint, respectively. Compared with the flange breadth  $B$ , seismic residual local deformations reach a relatively severe level. The maximum one comes to  $B/29$ , which may not be neglected for the post-earthquake serviceability of the steel bridge.

5.4 Seismic damaged areas

Fig. 15 shows the additional areas of plasticity caused merely by aftershock E. As it can be seen from the figure, areas of the newly generated plasticity by aftershock do not increase too much when consider the unrepaired damages. Actually, seismic damage areas are very concentrated, they are generally clustered at the joints or the boundary regions. Earthquake sequence can only affect the degree of plasticity, but it cannot affect the area size apparently.

5.5 Low-cycle fatigue evaluation

For a steel bridge under an earthquake sequence, the probability of low-cycle fatigue failure will increase greatly. The damage accumulation for a steel member can be better evaluated if strain concentration and stress state of the damage zone can be considered in a FE model. Fortunately, multi-scale hybrid model deals very well with these problems. As the most significant damage is observed at the intersection of the tie beam and the arch rib, the fracture failure prediction is performed in this part of the bridge.

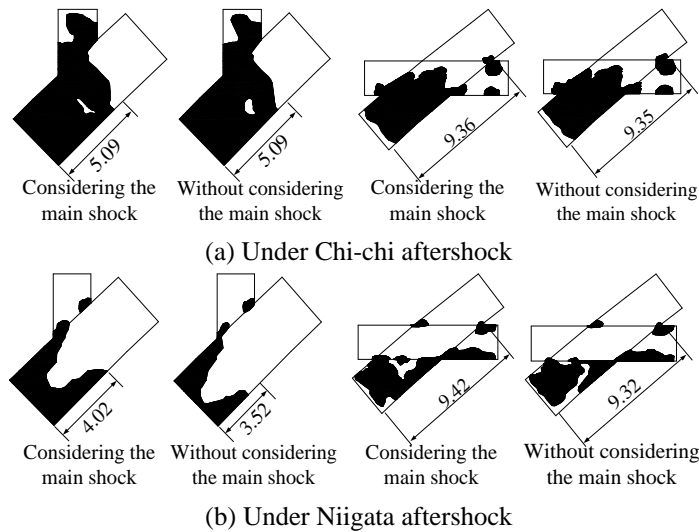


Fig. 15 Additional seismic damage areas caused by the aftershock only (Unit: m)

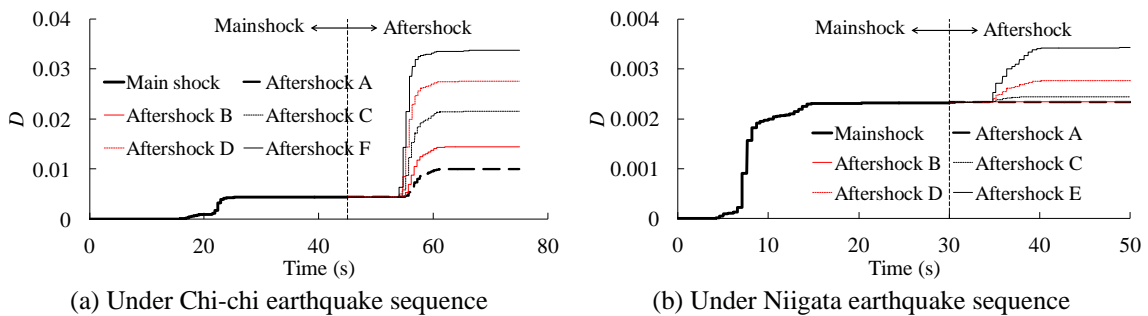


Fig. 16 The evolution of damage index  $D$  during the earthquake sequence

Fig. 16 shows the cumulative damage index  $D$  based on Miner's rule and Manson-Coffin relation according to Eq. (2). As it can be seen from the figure, the steel members of the structure haven't reached the critical damage under strong earthquake sequence.

Fig. 17 shows the cumulative damage index  $D$  of the damaged and undamaged structure caused by aftershock E only. The damage indexes under the two load cases are almost the same, which means the cumulative process for low-cycle fatigue damage is affected little by the unrepaired seismic damage.

In the dynamic calculation procedure, 5 Simpson integration points are specified through the thickness direction of the steel plates. The stress state at the surface of a steel plate is simple and clear since there is no extrusion stress. Based on the void growth theory, the stress state affects greatly the low-cycle fatigue index. Fig. 18 shows the stress triaxiality  $(\sigma_1 + \sigma_2 + \sigma_3) / 3\sigma_y$  and  $\sigma_m$ -history curves at the plate surface in the damage areas caused by Chi-chi earthquake sequence. The results show that steel material at the damaged area is alternatively under tensile and compressive states all through the earthquakes.

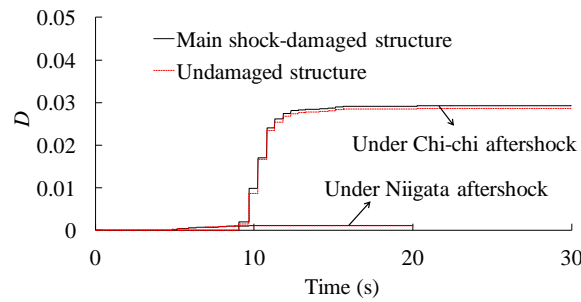


Fig. 17 Damage index  $D$  induced by aftershock only

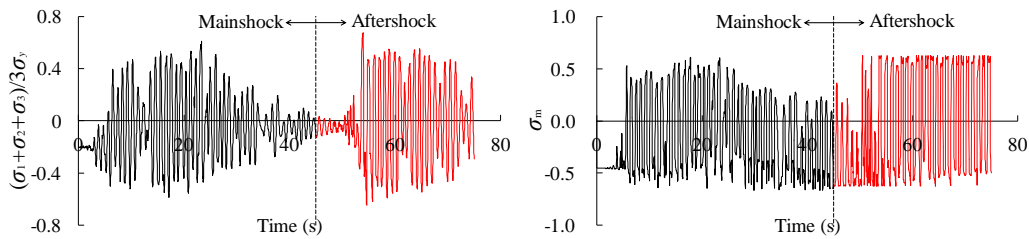
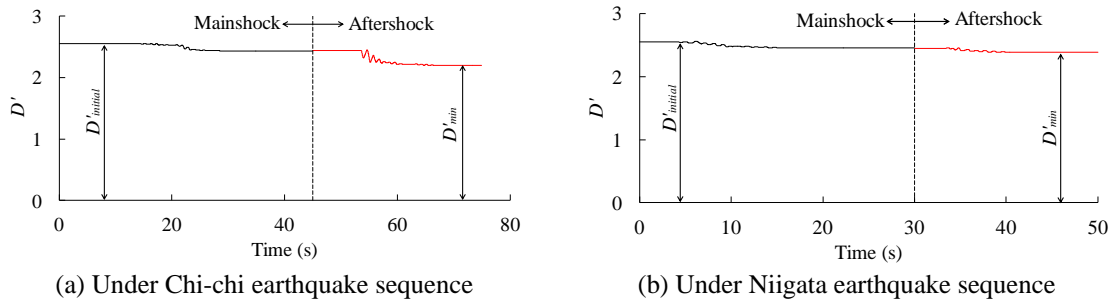


Fig. 18 Stress triaxiality in the damage area



(a) Under Chi-chi earthquake sequence

(b) Under Niigata earthquake sequence

Fig. 19 The evolution of damage index  $D'$  during the earthquake sequence

Table 1 Comparison of the indexes for low-cycle fatigue using different evaluation methods

Earthquake sequence	Maximum damage value/Critical value	
	$\frac{D_{\max}}{D_{\text{critical}}}$	$1 - \frac{D_{\min}}{D_{\text{initial}}}$
Chi-chi	3.4%	13.7%
Niigata	0.3%	6.4%

The damage evolution index during the main shock and the aftershock E in the damage area is obtained as shown in Fig. 19.  $\sigma_m$  is used to distinguish the tensile and compressive state according to Eq. (3), crack initiates when damage index  $D'$  becomes smaller than zero. The results indicate that the structure will not fail by low-cycle fatigue under the strong earthquake sequences.

In order to compare the evaluations of low-cycle fatigue damage, Table 1 lists the ratio of the maximum damage development and the critical value corresponding to Fig. 16 and Fig. 19. As it can be seen, the Chi-chi earthquake sequence causes more severe seismic damage than the Niigata earthquake sequence does. The damage extents predicted by different evaluation methods are not quite the same.

## 6. Conclusions

In this paper, real main shock-aftershock sequences records were taken as the input ground motions. Nonlinear time-history dynamic analysis of a steel arch bridge using fine multi-scale hybrid model was conducted. The influence of the unrepaired damage on the earthquake resistance of the steel arch bridge was studied carefully. Low-cycle fatigue failure of the steel bridge was predicted based on different theories. Some important conclusions can be drawn as follows.

- The unrepaired seismic damage has little impact on the overall displacement response, which indicates the overall stiffness of a steel bridge is not affected.
- The unrepaired seismic damage affects somehow the strain response of a steel structure under the aftershock. However, the increments of both the equivalent plastic strain and the strain response caused by the unrepaired damage are less than 10% in most cases.
- The unrepaired damage will increase the residual local deformation of the steel plate. Dynamic analysis of the steel arch bridge shows that the unrepaired damages enlarged the residual local deformation by 13.4% and 7.8% for the arch spring and the intersection joint, respectively.
- The unrepaired main shock-induced damage affects very slightly the area size of plasticity on a steel bridge under an aftershock. The seismic damage areas of a steel bridge are very concentrated, and they are generally clustered at the joints or near the boundary regions.
- According to different evaluation methods, the steel bridge is hardly to fail caused by low-cycle fatigue under strong earthquake sequence. The damage extents predicted by different evaluation methods are not quite the same.
- The low-cycle fatigue damage indexes of the steel bridge with and without seismic damage are almost the same, which means the cumulative process for low-cycle fatigue damage is affected little by the unrepaired seismic damage.

For future work, some material damage indexes may be introduced to the constitutive model of the structural steel. Thus, the degradation of seismic resistance for a steel bridge undergoing

earthquake sequence can be evaluated more accurately.

## Acknowledgments

The work described in this paper was substantially supported by the grant from the National Natural Science Foundation of China (No. 51378460), which is gratefully acknowledged by the authors.

## References

- Alliard, P.M. (2006), "Mainshocks and aftershocks sequences database", <http://www.polymtl.ca/structures/en/telecharg/index.php>.
- Amadio, C., Fragiacomio, M. and Rajgelj, S. (2003), "The effects of repeated earthquake ground motions on the non-linear response of SDOF systems", *Earthq. Eng. Struct. Dyn.*, **32**(2), 291-308.
- American Association of State Highway and Transportation Officials (2011), *AASHTO Guide Specifications for LRFD Seismic Bridge Design*, 2nd Edition.
- California Department of Transportation (2010), *Caltrans seismic Design Criteria*, Version 1.6.
- Chen, K.C., Huang, B.S., Wang, J.H. and Yen, H.Y. (2002), "Conjugate thrust faulting associated with the 1999 Chi-Chi, Taiwan, earthquake sequence", *Geophys. Res. Lett.*, **29**(8), 118-1-4.
- Chen, W.F. and Duan, L. (2014), *Bridge engineering handbook, Second edition: Seismic design*, CRC Press.
- Chi, W.M., Kanvinde, A.M. and Deierlein, G.G. (2006), "Prediction of ductile fracture in steel connections using SMCS criterion", *J. Struct. Eng.*, **132**(2), 171-181.
- Chinese Ministry of Communications (2008), *JTG/T B02-01-2008 Guidelines for Seismic Design of Highway Bridges*, Beijing: People's Communication Press.
- Faisal, A., Majid, T.A. and Hatzigeorgiou, G.D. (2013), "Investigation of story ductility demands of inelastic concrete frames subjected to repeated earthquakes", *Soil Dyn. Earthq. Eng.*, **44**(1), 42-53.
- Ge, H.B. and Luo, X.Q. (2011), "A seismic performance evaluation method for steel structures against local buckling and extra-low cycle fatigue", *J. Earthq. Tsunami*, **5**(2), 83-89.
- Ge, H.B. and Kang, L. (2012a), "A damage index-based evaluation method for predicting the ductile crack initiation in steel structures", *J. Earthq. Eng.*, **16**(5), 623-643.
- Ge, H.B., Chen, X. and Kang, L. (2012b), "Demand on stiffened steel shear panel dampers in a rigid-framed bridge pier under repeated seismic ground motions", *Adv. Struct. Eng.*, **15**(3), 525-546.
- Ge, H.B., Kang, L. and Hayami, K. (2013), "Recent research developments in ductile fracture of steel bridge structures", *J. Earthq. Tsunami*, **7**(3), 132-141.
- Ge, H.B. and Kang, L. (2014), "Ductile crack initiation and propagation in steel bridge piers subjected to random cyclic loading", *Eng. Struct.*, **59**, 809-820.
- Japan Meteorological Agency (2004), <http://www.jma.go.jp/index.html>.
- Japan Road Association (2002), *Specifications for Highway Bridges, Part V: Seismic Design*, Maruzen.
- Kakiuchi, T., Kasai, A., Inagaki, S., Fujiwara, Y. and Usami, T. (2009), "Seismic performance evaluation of steel continuous bridges with rigid superstructure-pier connections", *J. Struct. Eng.*, *JSCE*, **55A**, 564-572. (in Japanese)
- Kanvinde, A.M. and Deierlein, G.G. (2007), "Cyclic void growth model to assess ductile fracture initiation in structural steels due to ultra-low cycle fatigue", *J. Eng. Mech.*, ASCE, **133**(6), 701-712.
- Kim, K.H., Chen, K.C., Wang, J.H. and Chiu, J.M. (2010), "Seismogenic structures of the 1999 Mw 7.6 Chi-Chi, Taiwan, earthquake and its aftershocks", *Tectonophysics*, **489**(1), 119-127.
- Kiran, R. and Khandelwal, K. (2015), "A micromechanical cyclic void growth model for ultra-low cyclic fatigue", *Int. J. Fatig.*, **70**, 24-37.

- Li, Q. and Ellingwood, B.R. (2007), "Performance evaluation and damage assessment of steel frame buildings under main shock-aftershock earthquake sequences", *Earthq. Eng. Struct. Dyn.*, **36**(3), 405-427.
- Li, Y., Song, R. and Lindt, J.W.V.D. (2014), "Collapse fragility of steel structures subjected to earthquake mainshock-aftershock sequences", *J. Struct. Eng.*, **140**(12), 04014095-1-10.
- Liao, F.F., Wang, W. and Chen Y.Y. (2012), "Parameter calibrations and application of micromechanical fracture models of structural steels", *Struct. Eng. Mech.*, **42**(2), 153-174.
- Sakai, K. and Murono, Y. (2014), "Fundamental study on evaluation of main shock-aftershock ground motions for seismic design", *J. Japan Soc. Civ. Eng. Ser A1, JSCE*, **70**(4), I 644-I 653. (in Japanese)
- Sunasaka, Y. and Kiremidjian, A.S. (1993), "A method for structural safety evaluation under mainshock-aftershock earthquake sequences", Report No. 105, The John A. Blume Earthquake Engineering Center, United States.
- Tang, Z.Z., Xie, X., Wang, Y. and Wang, J.Z. (2014), "Investigation of elasto-plastic seismic response analysis method for complex steel bridges", *Earthq. Struct.*, **7**(3), 333-347.
- Tang, Z.Z., Xie, X., Wang, T. and Wang, J.Z. (2015), "Study on FE models in elasto-plastic seismic performance evaluation of steel arch bridge", *J. Constr. Steel Res.*, **113**, 209-220.
- Usami, T., Lu, Z.H. and Ge, H.B. (2005), "A seismic upgrading method for steel arch bridges using buckling-restrained braces", *Earthq. Eng. Struct. Dyn.*, **34**(4-5), 471-496.
- Usami, T. and Ge, H.B. (2009), "A performance-based seismic design methodology for steel bridge-systems", *J. Earthq. Tsunami*, **3**(3), 175-193.
- Vamvatsikos, D. and Cornell, C.A. (2004), "Applied incremental dynamic analysis", *Earthq. Spectra*, **20**(2), 523-553.
- Xie, X., Lin, G., Duan, Y.F. and Wang, Y.Z. (2012), "Seismic damage of long span steel tower suspension bridge considering strong aftershocks", *Earthq. Struct.*, **3**(5), 767-781.
- Yamao, T., Tsujino, Y. and Wang, Z.F. (2010), "Dynamic behavior and seismic retrofitting method for half-through steel arch bridges subjected to fault displacement", *ARCH'10-6th International Conference on Arch Bridges*, Fuzhou, China.
- Yeo, G.L. and Cornell, C.A. (2009), "A probabilistic framework for quantification of aftershock ground-motion hazard in California: Methodology and parametric study", *Earthq. Eng. Struct. Dyn.*, **38**(1), 45-60.
- Zhang, S., Wang, G. and Sa, W. (2013), "Damage evaluation of concrete gravity dams under mainshock-aftershock seismic sequences", *Soil Dyn. Earthq. Eng.*, **50**(1), 16-27.
- Zhao, B. and Taucer, F. (2010), "Performance of infrastructure during the May 12, 2008 Wenchuan earthquake in China", *J. Earthq. Eng.*, **14**(4), 578-600.
- Zhao, E.N. and Qu, W.L. (2014), "Multi-scale elastoplastic dynamic analysis of steel frame welded connections under strong earthquake excitation", *Appl. Mech. Mater.*, **501**, 1604-1608.